Print-Light-Synthesis of Gold Thin Film Electrodes for Electrochemical Sensing

*Emanuela Maiorano, Stefano Gianvittorio, Massimiliano Lanzi, Domenica Tonelli, Horst Pick, and Andreas Lesch**

The one-step fabrication of gold films by inkjet printing of a gold precursor ink and its photochemical reduction by exposure to UV light is presented. Inkjet printing creates on a substrate with high control micrometer-thin reaction volumes in which upon direct high-intensity light irradiation, the gold precursor reduces to pure and well-adhered Au particles, while all other ink components escape in the gas phase, without the need for any further post-treatment. The Au precursor ink does neither contain stabilizing agents, such as polymers or surfactants, nor sacrificial compounds, such as photoinitiators, to initiate and accelerate the reduction. This economic and green process is known as Print-Light-Synthesis (PLS) and is herein used to create gold patterns of thin compact Au films and separated Au nanoparticles. Gold loadings are in the µg cm^{-2} range and precisely controlled, thanks to the inkjet printing parameters. The gold films are characterized by spectroscopic and electrochemical methods. Finally, the applicability of Au films as electrochemical sensors is demonstrated for the detection of 1,4-butanediol in comparison to a commercial screen-printed Au electrode. The PLS Au electrode shows a 20 times higher sensitivity and opens new possibilities for disposable electrode production.

1. Introduction

The low-cost, large-scale fabrication of thin films of conventional, as well as advanced materials, is of large interest in many fields of applications including sensors, energy conversion, energy storage, and electronics.[1] Many efforts have been made to develop technologies suitable for the fabrication of thin and thick metal films, which include photolithography, screen printing, and inkjet printing. Ink-based deposition techniques, being one form of additive manufacturing, are of great interest due to their low production and material costs. Screen-printed sensors are prepared in large quantities and available at reasonably low costs, which is attractive for research, as well as for professional use, such as in diagnostics. In most approaches that involve inks, the fabrication of metal films is a multi-step process. Au nanoparticles (NPs) must first be synthesized, which is followed by the preparation of an ink that must fulfill the rheological requirements of the available printer or ink deposition machine. After the printing process, the deposited Au NP ink is first dried and thereafter exposed to a thermal post-treatment at elevated temperatures (generally between 300 and 500 °C for Au) in order to evaporate the ink solvents, to degrade and evaporate ink-stabilizing agents, such as polymers and surfactants, and to sinter the Au particles in order to create a conductive film.[2] High-temperature processes are energy-intensive and room-temperature methods get more in the focus.[3] One approach is "reactive printing," in which first a metal salt is printed and thereafter a second ink containing a reducing agent (e.g., NaBH$_4$ or antioxidants) that reduces the metal cation to the metal with oxidation state zero.[4] This requires, however, wet chemistry and washing of the printed film after the reduction process has finished. In another approach, metal precursor solutions are deposited and photochemically reduced to the metal.[5] This works well for elements with high reduction potential, such as gold ($E^\circ_{Au3+/Au0}$ = +1.5 V vs SHE). However, in order to accelerate or even realize the reduction of Au precursors on reasonable time scales, it might be necessary to add reducing agents[3b] or to use photocatalytic supports such as TiO$_2$.[6] For the fabrication of gold patterns based on gold precursor inks, a few methods have been proposed, including

E. Maiorano, S. Gianvittorio, M. Lanzi, D. Tonelli, A. Lesch
University of Bologna
Department of Industrial Chemistry "Toso Montanari"
Viale del Risorgimento 4, Bologna 40136, Italy
E-mail: andreas.lesch@unibo.it
E. Maiorano, H. Pick
Ecole Polytechnique Fédérale de Lausanne (EPFL)
Environmental Engineering Institute
GR-LUD
School of Architecture
Civil and Environmental Engineering
EPFL Station 2, Lausanne 1015, Switzerland

polymer-assisted photochemical deposition,[7] laser projection printing,[8] digital light processing,[9] direct laser writing,[10] anion-assisted photochemical deposition,[3b] and inkjet printing with subsequent high-temperature thermal precursor decomposition[11] or plasma treatment.[12] Recently, the rapid synthesis of films and coatings containing metals, metal oxides, and alloys based on the combination of an inkjet printer and a high-intensity flash lamp (i.e., photonic curing or intense pulsed light irradiation) has been introduced by Lesch as Print-Light-Synthesis (PLS).[13] Pt nanostructures and nanoparticles were synthesized on indium tin oxide-coated glass slides. Thereafter, the concept has been extended to the fabrication of thin films of Ni and NiFe nanocatalysts[14] and Prussian Blue.[15]

Many light-assisted printing processes for the production of thin metal films, in reality, are sequential, because the irradiation step cannot be performed simultaneously with the printing. For instance, using photonic curing as the source of high-intensity pulsed light cannot be integrated into the printhead of an inkjet printer due to its bulky dimensions. Therefore, photonic curing is carried out subsequently to printing or as an intermediate step while temporarily interrupting a longer printing process. An alternative solution is to integrate a different light source into the printing device. This can be a small light guide transferring, for instance, UV irradiation from an external UV lamp into the printer.[16] In that case, the light guide, and thus the UV light, translates together with the inkjet printhead over the substrate enabling real simultaneous printing and photochemistry.

Au films find many applications as electrodes in disposable electrochemical sensors.[2c,17] Therefore, end users of such sensors are research laboratories and clients in the sensor industry. The research and use of electrochemical sensors rely generally on commercially available electrodes, typically prepared by screen-printing or photolithography, as not all laboratories are equipped with state-of-the-art microfabrication techniques. The implementation of different materials in one type of sensor might further require the use of different material deposition techniques, one optimized for each material. Commercial electrodes, not limited solely to Au, are generally used as received. Optionally, the surface of the working electrode (WE) is chemically modified, for instance with hydrogels or catalytically active nanoparticles. The acquisition of such sensors creates costs for the laboratory, does not offer flexibility regarding electrode materials, dimensions, and designs, and often presents electrochemical properties in terms of measurement stability, sensibility (affected by the material used and cleanliness of the fabrication process), and sensor-to-sensor reproducibility that do not always meet the expectations of the users.

Therefore, we present a simple, rapid, and sustainable way of fabricating on large-scale gold electrodes with controllable Au loadings and flexible pattern designs. The microfabrication process is based on the highly controlled deposition of a gold precursor ink with immediate exposure to UV light creating simultaneous printing and photodeposition of solid gold patterns. The presented approach represents a novel economic version of the PLS by using a low-cost light source. The requirements of the ink and optimization of printing parameters are discussed, which is followed by a detailed spectroscopic and electrochemical characterization of the PLS Au films. The applicability of the as-obtained gold electrodes as sensors is demonstrated by various electro-

analytical measurements and the superior behavior of the PLS gold electrodes versus typical commercial screen-printed Au electrodes is presented.

2. Print-Light-Synthesis of Gold Films

Print-Light-Synthesis of thin gold films is the result of the controlled deposition of a thin liquid layer of a gold precursor ink containing $[AuCl_4]^-$ and the photochemically-induced reduction of $[AuCl_4]^-$ to Au^0. This is technically realized by using a hybrid system composed of an inkjet printer and a UV lamp (**Figure 1**, details in Section S1, Supporting Information). Apart from the gold salt and mixture of solvents (i.e., water, isopropanol, and 1,2-propanediol) the ink does not contain any stabilizing agents or surfactants. The volume of ink deposited is controlled by the number of droplets per area (i.e., droplets per in. – dpi). This creates minor reaction volumes, in which the photochemical reactions take place upon irradiation with intensive light of proper wavelengths. The substrate can optionally be heated up to 60 °C simply to facilitate the evaporation of the ink solvents while secondary products of the photochemical reduction of the gold precursor lead to the formation of gaseous or easily evaporable compounds such as H_2O, Cl_2, HCl, ROH, and CO_2 (R is an organic residue such as CH_3-CH_2-). Therefore, only pure Au is found on the substrate while all other elements are removed during PLS. The loading of the gold precursor on the substrate (i.e., the mass of deposited Au per substrate area), controlled by the ink composition and dpi number, determines which type of gold coating is obtained during PLS. Considering a fixed precursor concentration, high dpi numbers (i.e., high gold loading on the substrate) result in compact gold films that are conductive even when deposited on insulators (Figure 1a), while low dpi numbers (i.e., low gold precursor loadings) result in coatings of separated gold nanoparticles (Figure 1b).

First, the photochemically induced reduction of $[AuCl_4]^-$ is demonstrated by irradiation of a vial filled with the inkjet ink containing thus the gold precursor and solvent mixture. With a standard redox potential of $E°_{AuCl4-/Au(s)} = +1.0$ V vs SHE, the gold precursor can be reduced under relatively mild reducing conditions, here as a result of the absorption of UV light. The photochemical reduction of $[AuCl_4]^-$ by using irradiation with light of different wavelengths, irradiation times, and intensities has been widely studied in the literature and the mechanistic pathways under various experimental conditions are well established.[18] Key reactions are the UV light-induced generation of reducing species, such as the hydrated electron e^-_{aq}, which can be formed by the interaction of electromagnetic radiation of sufficiently high intensity with water, as well as with chloride anions (details in Section S2, Supporting Information).[18a,b,19] The hydrated electron is an extremely short-living species (lifetime of up to a few hundred nanoseconds in pure water) that without stabilization regenerates water, or in presence of electron donors, like alkali metals, reduces water to hydrogen.[20] However, it can also be a strong reducing agent for other species in the solution. The reduction of cationic Au species to Au^0 according to Equation (1) has been reported.

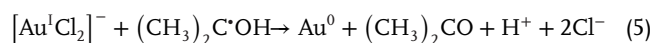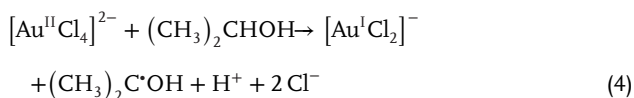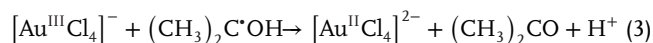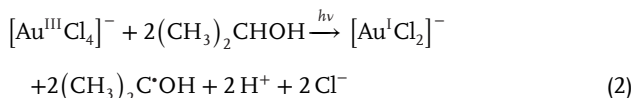$$[Au^{III}Cl_4]^- + 3\,e^-_{aq} \rightarrow Au^0 + 4\,Cl^- \tag{1}$$
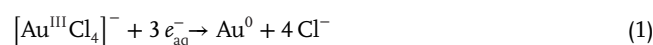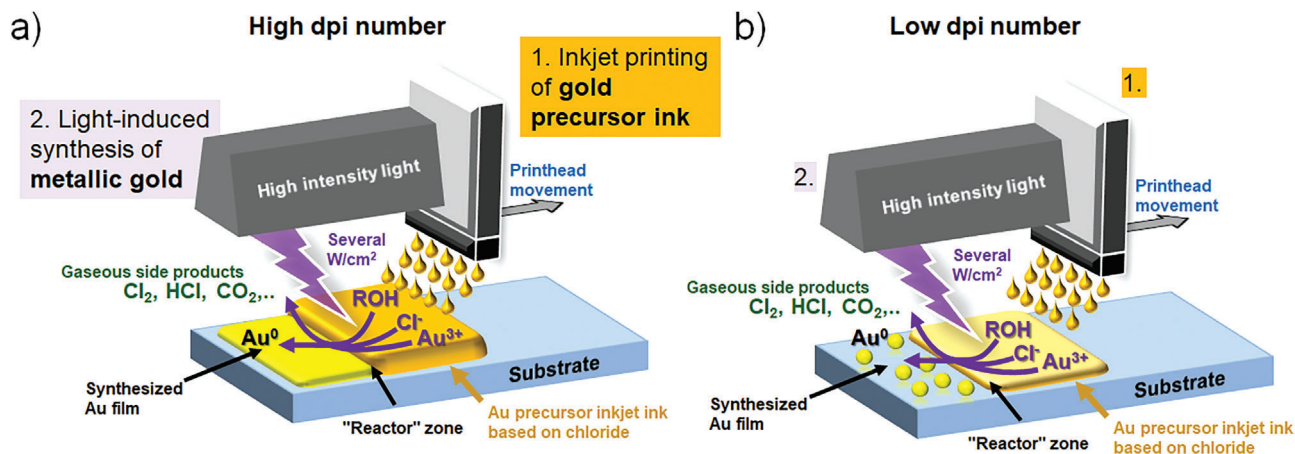
Figure 1. Schematic representation of Print-Light-Synthesis for the patterning of thin Au films using a piezoelectric inkjet printer in combination with a high-intensity UV light source. The printhead of the inkjet printer was customized to enable the integration of the high-intensity light source, generating thus a "PLS head." A gold precursor ink is printed as a thin liquid layer of micrometer thickness and immediately exposed to UV irradiation reducing the Au^{III} precursor to Au^0 while generating only evaporated and gaseous side products. When using a fixed Au precursor concentration in the ink two situations can be achieved: a) a high number of droplets per in. (dpi) of deposited Au precursor ink results in conductive gold films. b) A low dpi number of deposited Au precursor ink results in a film of separated Au nanoparticles.
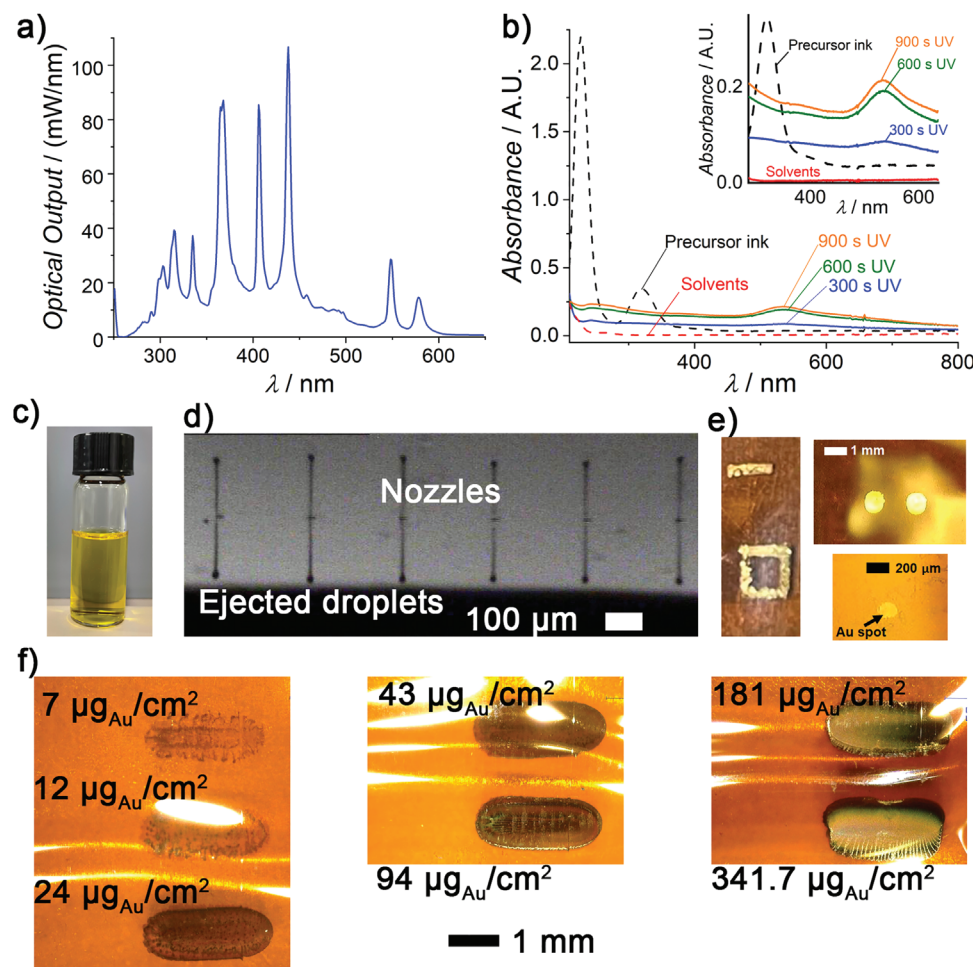
The hydrated electron can generate also hydrogen atoms, hydroxyl radicals, and in particular, H_2O_2, which are highly reactive reducing species, but quickly scavenged for instance by alcohols in the reaction mixture, herein, isopropanol and 1,2-propanediol.[21]

Moreover, isopropanol, irradiated with UV light, and especially, when having been transformed into its radical, acts as a strong reducing agent reducing the gold species by several cascade redox reactions,[18a,21b] from which four most likely occuring ones are demonstrated in Equations (2)–(5) (details in Section S2, Supporting Information)

$$[Au^{III}Cl_4]^- + 2(CH_3)_2CHOH \xrightarrow{h\nu} [Au^ICl_2]^-$$
$$+2(CH_3)_2C^\bullet OH + 2H^+ + 2Cl^- \quad (2)$$

$$[Au^{III}Cl_4]^- + (CH_3)_2C^\bullet OH \rightarrow [Au^{II}Cl_4]^{2-} + (CH_3)_2CO + H^+ \quad (3)$$

$$[Au^{II}Cl_4]^{2-} + (CH_3)_2CHOH \rightarrow [Au^ICl_2]^-$$
$$+(CH_3)_2C^\bullet OH + H^+ + 2Cl^- \quad (4)$$

$$[Au^ICl_2]^- + (CH_3)_2C^\bullet OH \rightarrow Au^0 + (CH_3)_2CO + H^+ + 2Cl^- \quad (5)$$

Gold atoms in solution assemble gold clusters that can act as seeds for gold precursor adsorption and further Au^0 formation forming eventually Au nanoparticles (Section S2, Supporting Information). **Figure 2**a shows the emission spectrum of the UV lamp utilized in this work. The typical peaks of the various emission lines of mercury can be clearly seen, as well as continuous emission of lower intensity between about 200 nm and 600 nm. The outlet of the UV lamp is connected to a liquid light guide

that transports the light and emits at its tip a focused spot of UV light of 5 mm diameter, irradiating therefore only a part of the vial. The behavior of this macroscopic volume of ink differs substantially from the microvolumes created by inkjet printing during PLS. Further, the glass of the vial will absorb part of the UV light reducing the efficiency of the process. It can therefore be expected that the time required for complete gold reduction in stirred bulk solution will be longer than for thin layers of the ink. Figure 2b shows the UV/VIS absorption spectra of the gold inkjet ink before and after different irradiation periods, recorded in a quartz glass cell. The gold ink shows two characteristic absorption peaks at about 220 nm and 320 nm, respectively, which correspond well with the emission wavelengths of the UV lamp. The UV lamp is thus suitable to induce the photochemical reduction of the Au precursor. The ink solvents, that is, a mixture of water, isopropanol, and 1,2-propanediol show negligible absorption over all wavelengths. However, both isopropanol and 1,2-propanediol can act as reducing agents accelerating the reduction of $[AuCl_4]^-$. It can be seen in the UV/VIS absorption spectra (Figure 2b) that the absorption peaks related to the gold precursor disappeared in all cases. A characteristic absorption peak for Au^0 can be seen at 534 nm. The intensity of the peak increases with exposure time due to the continuous formation of Au NPs. As the ink does not contain size-stabilizing agents, the resulting particle size is a result of the equilibrium condition reached during the process. After having confirmed that the UV light source in combination with the gold precursor ink is suitable to synthesize Au^0, the inkjet printability of the ink was investigated. The concentration of the gold precursor salt was generally 30 $mg_{[AuCl4]^-}$ mL^{-1} (Figure 2c). The inks could be stored for several months in the dark without showing signs of degradation in terms of visible precipitates, discoloration, or characteristic absorption peaks in the UV/VIS spectra (Section S3, Supporting Information). Stable jetting was observed over months thanks to the adjusted viscosity and surface tension, as well as the absence of nanoparticles or other compounds that could cause nozzle clogging (Figure 2d).

**ADVANCED
SCIENCE NEWS**

www.advancedsciencenews.com

**ADVANCED
MATERIALS
TECHNOLOGIES**

www.advmattechnol.de

Figure 2. a) Emission spectrum of the light irradiated by the mercury-based UV lamp utilized in this work. b) UV/VIS absorption spectra of bulk solution of the Au precursor inkjet ink inside a glass vial after different exposure times to UV irradiation. c) Au precursor inkjet ink. d) Ejection of the ink from six consecutive nozzles of the inkjet printer used in this work operating with piezoelectric actuation (note: the photo was taken directly after ejection of the droplets when the tail is still visible. After 1 mm of falling, the ejected droplets formed spheres). e) Exemplary gold patterns printed on polyimide (left panel: lines and rectangular frame; upper right panel: circular Au patterns; lower right: Au spot). f) Photographs of seven gold patterns of identical theoretical dimension, but with increasing Au loading, deposited using PLS.

The Ohnesorge Oh number was used as a numeric indicator to evaluate the general jettability of the ink.[22] The reciprocal of Oh has been introduced in literature as the dimensionless Z number, defined as $Z = Oh^{-1} = (\gamma \times \rho \times a)^{0.5}/\eta$ where γ, η, and ρ are the surface tension, viscosity, and density of the ink, respectively. The quantity a represents a characteristic length, which in this case is the diameter of the nozzle orifice, that is, 21.5 µm. The ternary solvent mixture used as ink basis fulfilled three main characteristics to obtain stable jetting: water was added to dissolve the Au precursor salt, isopropanol to obtain a suitable γ, and 1,2-propanediol to reach a proper η. The calculated Z value was 5.6, which matches the predicted printability range of $1 < Z < 10$.[22] The presence of 1,2-propanediol has another advantage, which is caused by its slow evaporation rate. In that way, the drying time of the printed layer of precursor ink was extended assuring that a liquid layer was exposed to the light rather than a precipitated salt.[13] The absence of particles in the ink allowed stable printing for hours without the necessity to clean the nozzles, which is usually required for many nanoparticle-containing inks that cause

often clogging of the nozzle orifices. In worst cases, the nozzle orifices can be irreversibly blocked by precipitated and aggregated nanoparticles. Nozzle cleaning in general is done by purging (i.e., the excessive release of ink under pressure from the nozzles to flush away all possible precipitates), which can result in notable losses of ink volume. The use of the purge-free gold precursor ink in this work demonstrated therefore a printing yield of 100%, thus without material loss.

Gold patterns of various shapes, such as gold spots and circular gold patterns of 200 µm and 1 mm diameter, respectively, as well as gold bands and frames, were prepared by PLS on polyimide (PI) foil (Figure 2e). In order to guarantee complete conversion of the Au precursor during each printing pass (i.e., one single PLS head translation over the substrate), the printing speed must be limited. It has been found that the translation rate of the PLS head should be less than 5 mm s^{-1}. When faster printing speeds were applied, traces of gold chloride were found for single printing passes. With optimized printing speed, no further treatment of the printed patterns was required and the Au films could be

**ADVANCED
SCIENCE NEWS**

www.advancedsciencenews.com

**ADVANCED
MATERIALS
TECHNOLOGIES**

www.advmattechnol.de

immediately used. The amount of Au deposited was controlled by the printing parameters, precisely by the programmable dpi number (Figure 2f). Alternatively, the concentration of the Au precursor can be changed, but it is certainly more convenient and faster to change the printing parameters than the ink. The mass of gold deposited per area was calculated based on the ink volume printed per pattern. The droplet volume was estimated as (11.4 ± 0.7) pL ($N = 3$). It was obtained by analyzing the images of individual spherical droplets, taken with the video camera integrated with the printer, after 1 mm of falling post droplet ejection. The Au pattern dimensions were measured with a digital microscope and digital image analysis tools. Seven different gold loadings were then prepared by printing one layer of ink (i.e, only one droplet was deposited per coordinate). As can be seen from the optical micrographs, above 43 μg_{Au} cm^{-2} the gold patterns appear as homogeneous surfaces. Above 181 μg_{Au} cm^{-2} however (for a one-layer printing process), the patterns start to lose resolution due to the extended volume of ink starting to spread over the edges of the main pattern. The photochemically induced reduction of Au^{III} during PLS takes place in very confined reaction volumes on the substrate, created by inkjet printing of the precursor ink. Depending on the dpi number, the estimated thickness of the reaction volumes, not considering immediate solvent evaporation, was between 6 μm and 110 μm for 270 and 2505 dpi, respectively. These confined reaction volumes facilitate the deposition of Au^0 onto the substrate surface with good adhesion. In order to increase the Au loading, one possibility is to repeat the printing process and printing in that way various layers on top of each other.

2.1. Electron Microscopic and Spectroscopic Characterization of Gold Films Prepared by Print-Light-Synthesis
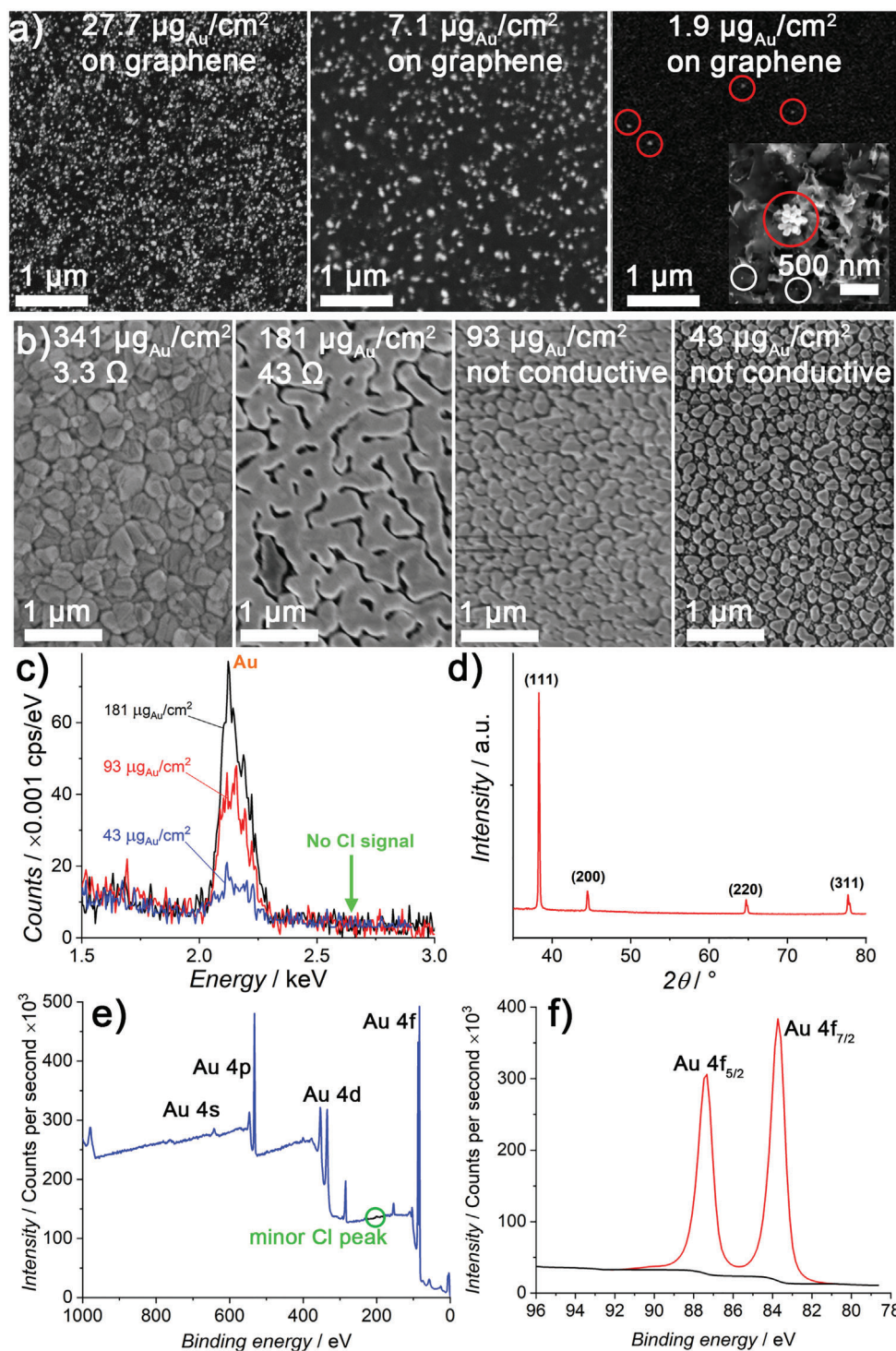
Two types of gold-based films were fabricated in this work with the aim to be used as electrodes in electroanalytical sensors. One type required the deposition of individual Au NPs onto a conductive support, i.e., inkjet-printed graphene, to fabricate Au NP/graphene electrodes (**Figure 3**a). Individual Au particles were expected from the microscopic investigation vide supra to appear with gold loadings below 43 μg_{Au} cm^{-2}. Three dpi numbers were applied and three electrodes were prepared. The SEM micrographs of these three electrodes demonstrate the increasing mass of Au from 1.9 to 7.1 and 27.7 μg_{Au} cm^{-2} by the increasing number of Au NPs (bright spots on graphene that appear dark). Interestingly, the mean particle size of the Au NPs on graphene decreases with increasing precursor loading during printing (Figure 3a, left and central panels). In fact, apart from small Au nanoparticles (white circles), aggregates of gold nanoparticles are observed with the lowest Au loading (inset in Figure 3a, right panel, red circles). These results demonstrate that the PLS parameters, using only one Au precursor ink, can influence the synthesis of Au NPs on a conductive support. Thereafter, PLS was performed on insulating substrates, such as polyimide foil, with the aim to fabricate conductive Au films (Figure 3b). With 43 and 93 μg_{Au} cm^{-2} larger Au particles were formed that showed poor percolation, which therefore resulted in nonconductive Au films. Increasing the Au loading to 181 μg_{Au} cm^{-2} resulted in percolation and partial sintering of Au particles gen-

erating a moderately conductive Au film (43 Ω, electrical conductivity measurements vide infra). Increasing the Au loading further increased the sintering rate and reduced the resistance of the gold film until reaching a compact, hole-free Au film with 341 μg_{Au} cm^{-2} and 3.3 Ω. During PLS, initial Au atoms and clusters also absorb UV light (see UV/vis spectrum vide supra). This might promote the reduction of the Au precursor preferably on excited Au^0, facilitating the growth of the first generated Au particles rather than creating new Au NPs. However, at this stage, this is a mechanistic proposition.
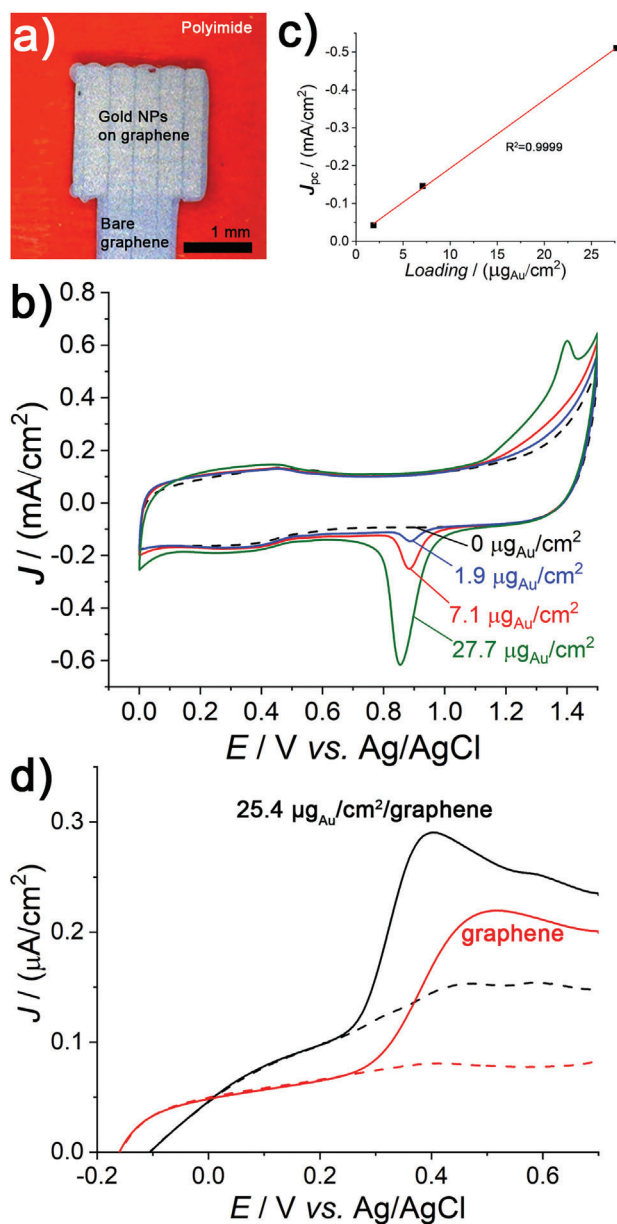
Energy-dispersive X-ray spectroscopy (EDS) was then performed to investigate whether the conversion of the gold precursor to Au^0 was complete. The main indicator for the completeness of the precursor conversion is the absence of the chlorine peak in the EDS spectrum. In fact, no chlorine peak was observed for samples with 43 to 86 and 181 μg_{Au} cm^{-2} while the peak related to gold increased according to the Au loading (Figure 3c). The XRD spectrum (Figure 3d) shows four characteristic peaks for the Au faces at diffraction angles 38.3° (111), 44.5° (200), 64.72° (220), and 77.71° (311). No peaks related to the Au precursors, that is, Cl-containing compounds were found. The lattice constant equal to (4.0741 ± 0.0007) Å, obtained by fitting with a cubic unit cell of Fm3m symmetry, was consistent with the literature. The mean isotropic domain size was refined to 46 nm. The XPS spectrum (Figure 3e) shows all common Au peaks as expected and only a minor signal for Cl at 200 eV. In the Au 4f region (Figure 3f), clear peaks for Au 4f7/2 and Au 4f5/2 are seen at 87.42 and 83.75 eV, respectively, with $\Delta = 3.67$ eV.

2.2. Electrochemical Performance of PLS Au Electrodes Prepared by Print-Light-Synthesis

As the PLS gold is preferably used by us as WE material for electrochemical sensors, the electrochemical performance of the PLS Au electrodes was evaluated by using cyclic voltammetry. First, the performance of PLS Au NP/graphene electrodes with three different Au loadings was investigated in 0.5 M H$_2$SO$_4$ and the results were compared with the bare graphene electrode (electrode blank). **Figure 4**a shows the micrograph of one exemplary graphene electrode (electrode area 2 mm × 2 mm) coated with 27.7 μg_{Au} cm^{-2}. The presence of Au had been verified by SEM (vide supra), but a yellowish coloration of the graphene surface can even be seen by the eye as well. The strip of bare graphene, seen at the bottom of the picture of the electrode used for electrical connection, was insulated with an inkjet-printed dielectric ink resulting in an active working electrode area of 4 mm^2. The resulting cyclic voltammograms (CVs) of the four tested electrodes are shown in Figure 4b. The electrode blank measurement (i.e., using the non-coated graphene electrode) shows over the entire potential window the typical broad CV shape for an electrode film composed of graphene. The broadening of the CV is caused by dominant capacitive currents that are caused by the charging and discharging of the electrical double layer. The capacitive contribution to the total recorded current is proportional to the real surface area of the electrode, which is influenced by the surface roughness and porosity of the graphene pattern. At about 1.3 V, the current starts to increase, which could be related to the evolution of oxygen through the electrochemical oxidation of water.

2202039 (5 of 12)

**ADVANCED
SCIENCE NEWS**

www.advancedsciencenews.com

**ADVANCED
MATERIALS
TECHNOLOGIES**

www.advmattechnol.de

Figure 3. a) SEM micrographs of patterns of Au nanoparticles on graphene realized by PLS with three different Au loadings. b) SEM micrographs of Au films on polyimide with different Au loadings as obtained by PLS. Resistance values measured in two-point-probe mode. c) EDS spectra of Au films with three different Au loadings, created by PLS on polyimide. The Au peak is indicated, as well as the theoretical position of the precursor salt anion. d) XRD spectrum of Au film obtained by PLS on polyimide. e) XPS spectrum of Au film on polyimide. f) XPS peaks related to Au 4f.

**ADVANCED
SCIENCE NEWS**

www.advancedsciencenews.com

**ADVANCED
MATERIALS
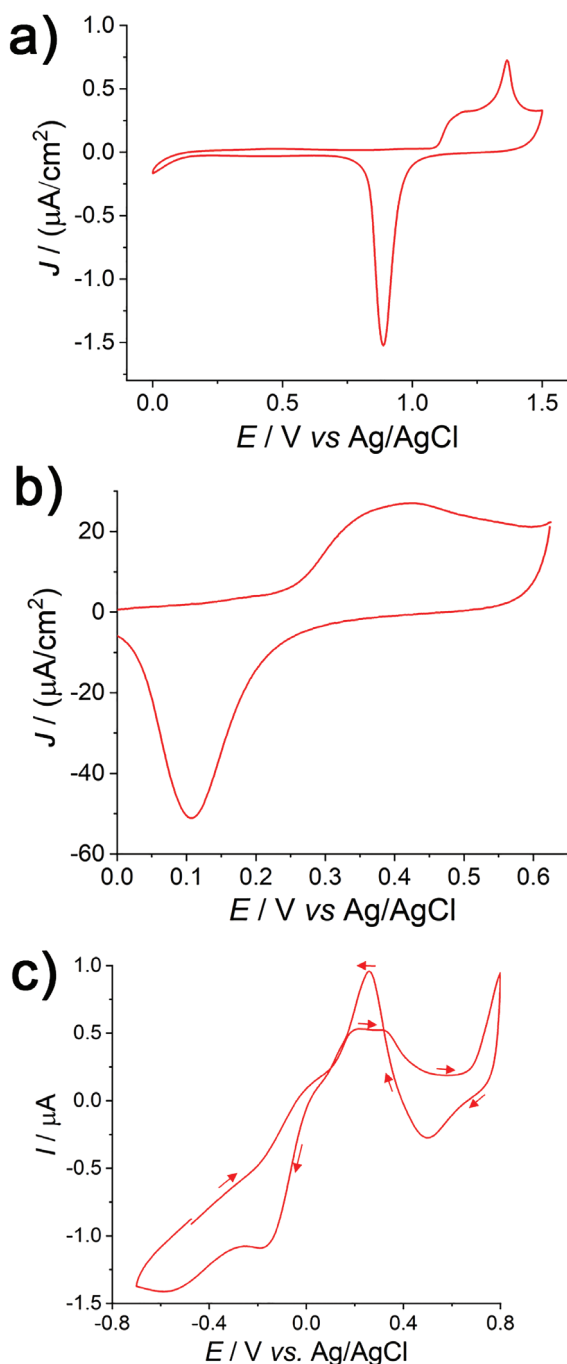TECHNOLOGIES**

www.advmattechnol.de

Figure 4. Electrochemical performance of PLS Au NP/graphene electrodes. a) Inkjet-printed graphene electrodes coated with different loadings of Au NPs as obtained by PLS. Polyimide was used as substrate. b) Cyclic voltammograms (CVs) of Au NPs, obtained by PLS, on inkjet-printed graphene electrodes, in comparison to the CV recorded with a bare graphene electrode (black dashed line). Au NP loadings were 1.9 (blue), 7.1 (red), and 27.7 μg_{Au} cm^{-2} (green), respectively. Measurements were performed in 0.5 M H_2SO_4 with a scan rate of 100 mV s^{-1}. c) Linear regression graph of the peak currents for the reduction of gold oxide as obtained during the CVs of (b), baseline-corrected, versus Au loading. d) LSVs for the detection of ascorbic acid comparing the performance of PLS Au NP/graphene electrode (25.4 μg_{Au} cm^{-2}, black curves) with a bare graphene electrode (right curve). The test solution with 1 mM ascorbic acid in 0.1 M $HClO_4$ (solid lines) and the blank (dashed lines) were measured with a scan rate of 100 mV s^{-1}.

With Au NPs deposited on graphene, the recorded current starts to increase already at about 1.1 V, leading even to an oxidation peak at about 1.3 V for the highest Au loading. This enhancement of current, which becomes more pronounced with increasing Au loading, is most likely due to the well-known formation of Au oxide. In the reverse scan, the reduction of the as-generated Au oxide takes place generating sharp reduction peaks at about 0.95 V. The reduction peak is absent in the CV recorded with the bare graphene electrode confirming the presence of Au on the graphene electrodes treated with PLS of Au. The height of the reduction peaks, determined by subtracting from all CVs the electrode blank (i.e., the curve obtained with the bare graphene electrode) was proportional to the Au loading (Figure 4c), resulting in an r^2 close to 1. This is an interesting outcome of PLS because it demonstrates that the increase of the total gold surface is proportional to the Au loading, which is controlled by the parameters used for inkjet printing. The advantages of the PLS Au NP/graphene electrodes for electroanalytical sensing were verified by detecting an antioxidant. Figure 4d shows the linear sweep voltammograms (LSVs) of the sample blanks (i.e., 0.1 M $HClO_4$, dashed lines) and of the test solution, which was 1 mM ascorbic acid in 0.1 M $HClO_4$ (solid lines). Covered with Au NPs, the graphene electrode shows a more pronounced slope and current peak for the oxidation of ascorbic acid. Both LSV features occur at a lower electrode potential compared to bare graphene, indicating thus an electrocatalytic effect for the electro-oxidation of antioxidants thanks to the PLS Au NPs.

Thereafter, the electrochemical performance of the thin conductive Au film electrodes on polyimide was evaluated in acidic and basic aqueous solutions. The Au film overlapped partially with an inkjet-printed Ag film for electrical connection. The Ag was insulated by inkjet printing of the dielectric ink. The CVs recorded in 0.5 M H_2SO_4 and 0.1 M KOH show the characteristic peaks and waves expected for Au. In 0.5 M H_2SO_4 (**Figure 5**a), the broad anodic signal starting from 1.05 V upward corresponds to the formation of Au oxides. Two minor and one large oxidation peak can be seen that can be correlated to the different Au faces. For instance, the large oxidation peak at 1.37 V is generally referred to as Au (111). This is in agreement with the pronounced diffraction peak for Au (111) in the XRD spectrum (vide supra). The large reduction peak at 0.89 V corresponds to the electrochemical reduction of Au oxide. Also in 0.1 M KOH (Figure 5b), the shape of the CV corresponds to the one generally reported for gold. Above 0.25 V, Au hydroxide ($AuOH_3$) formation sets in, while the reduction of gold hydroxide is observed at about 0.1 V. Notably, the Au films showed strong adhesion to the PI substrate over a broad range of pH values and under long immersion times (i.e., at least for hours) in solution. Au is further known to be a suitable electrode material for the electrochemical detection of alcohols and saccharides.[23] In particular, the detection of glucose has been studied at Au for many years. For instance, many so-called enzyme-less glucose sensors based on gold or gold/copper oxide composites have been proposed.[23c,24] Therefore, the response of a gold electrode to glucose can be used as an indicator for evaluating the applicability of the PLS Au film electrode. Glucose is generally detected at Au in pH ranges 7–12.[25] In fact, the CV in Figure 5c, recorded in phosphate-buffered solution at physiological pH (i.e., pH 7.4) containing 5 mM glucose, showed clearly the presence of glucose-related peaks. Working

**ADVANCED
SCIENCE NEWS**

www.advancedsciencenews.com

**ADVANCED
MATERIALS
TECHNOLOGIES**

www.advmattechnol.de

Figure 5. Basic electrochemical characterization of thin Au film electrodes prepared by PLS on polyimide foil. a) Cyclic voltammogram (CV) in 0.5 M H_2SO_4, scan rate 100 mV s^{-1}. b) CV in 0.1 M KOH, 10 mV s^{-1}. c) CV in 5 mM glucose in phosphate-buffered solution (pH 7.4), scan rate 20 mV s^{-1}, not degassed.

cose oxidation to gluconolactone sets in. The anodic currents at more positive potentials are most likely the result of the formation of gold hydroxide, which is inactive for the oxidation of glucose. In fact, Au(III) hydroxide is the preferred species in the pH range of 7–12 in that potential region according to the Pourbaix diagram.[25] Gold hydroxide is then reduced in the reverse scan at about 0.5 V (reduction peak), enabling again the adsorption of glucose and its electro-oxidation as demonstrated by the significant current increase reaching an anodic peak at 0.26 V. The process is more efficient when being carried out in alkaline media.[25] However, with the PLS Au film electrodes, glucose can be even detected under near-neutral conditions. The signals at potentials inferior to 0 V are due to the reduction of dissolved oxygen in the solution. The electrochemical detection of a specific analyte of interest with the PLS gold film electrode is discussed in detail in the following section.

2.3. Use of PLS Au Film Electrodes as Electrochemical Sensors

In order to perform electroanalytical measurements, the active area of the Au electrode must be reproducibly fabricated. In order to improve the resolution of the fabrication of Au films by PLS, a modification of the PLS procedure was performed. Improving the resolution of inkjet printing can be generally achieved by the avoidance of the lateral spreading of the ink over the substrate surface before the target ink components are solidified. The diameter of the UV spot, which exits the outlet of the light guide, is 5 mm and thus larger than the dimensions of the printed Au precursor pattern during one printing pass. Therefore, a larger area of polyimide absorbs the light that is directed at it during PLS (Section S3, Supporting Information). As well known, PI is a material of high thermal stability and is used as an electrical and thermal isolator. Due to its low thermal conductivity (≈0.18 W (m K)$^{-1}$), it can heat up upon continuous irradiation with proper wavelengths. When the thin polyimide foil is fixed to the metal vacuum chuck of the inkjet printer, the vacuum chuck can transport part of the generated heat immediately away from the PI and block in this way strong local heat generation (**Figure 6**a, upper panel). The transport of heat away from the reaction volume was then avoided by placing the PI substrate on the vacuum chuck of the printer using a spacer of 150 µm or 300 µm creating a space between the PI foil and the metal chuck of the printer that was filled with air. The air in that space impedes the transfer of the heat from the PI foil creating a region of local heat confinement just below the irradiated reaction volume. From the observations made, it is suggested that Au^0 formation is facilitated and ink spreading is reduced (Figure 6b), which can be seen from the obtained resolution of the printed patterns (Figure 6c,d). While with metal contact below the PI, the spreading of the ink perpendicular to the printing direction was above 1.35 mm leading to an elliptic total shape of the printed pattern, 0.51 mm, and a rectangular shape was reached when there was air below the substrate (the differences in ink spreading are indicated as two vertical double arrows). Thermal reduction of [AuCl$_4$]$^-$ at air is known as a three-step process generating Au^0 at about 300 °C, leading to gaseous or easily evaporable side products (Section S2, Supporting Information).[26] However, it is important to highlight that the conversion of the Au precursor into Au^0 in this work is not
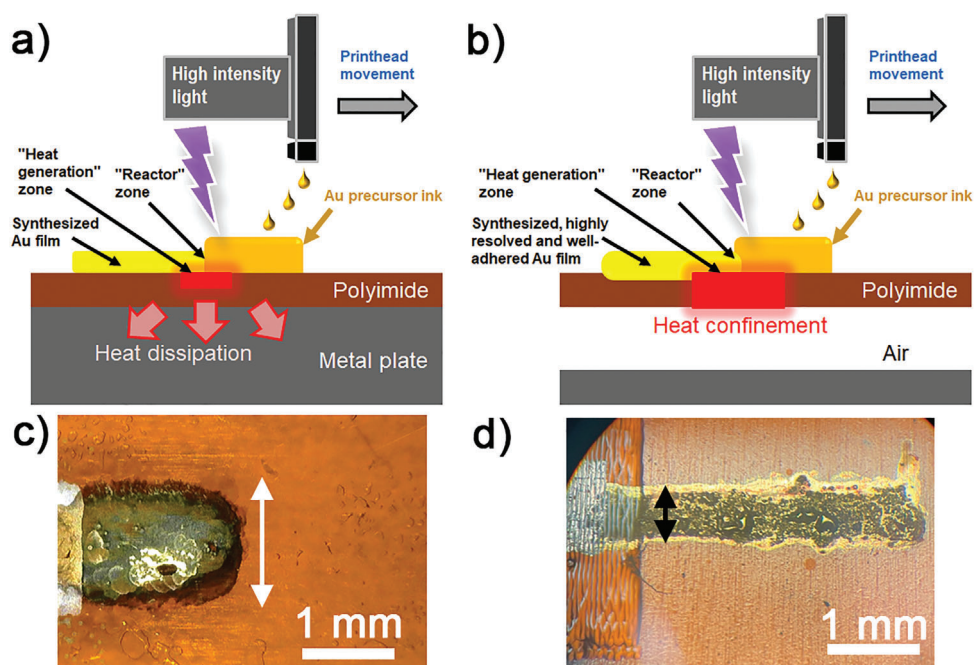
under physiological conditions has the advantage of not being obliged to manipulate the pH or the matrix of a sample solution. This is of interest when measuring, for instance, in body fluids or cell cultures. In the forward scan, starting from −0.5 V, the adsorption of glucose is seen by the oxidation wave between about 0.10 and 0.45 V as a result of dehydrogenation. Thereafter, glu-

ADVANCED
SCIENCE NEWS

www.advancedsciencenews.com

ADVANCED
MATERIALS
TECHNOLOGIES

www.advmattechnol.de

Figure 6. Optimized PLS to improve printing resolution by influencing the distribution and transfer of the heat locally generated by the absorption of UV light by polyimide. Notes: the lengths of the two Au patterns were different (2 mm in (b) and 4 mm in (c)) and the focus is made on the direction perpendicular to the printing direction. The direction of inkjet printing of the gold precursor ink was in both cases from left to right.

Table 1. Loading and electrical conductivity of Au films obtained by Print-Light-Synthesis.

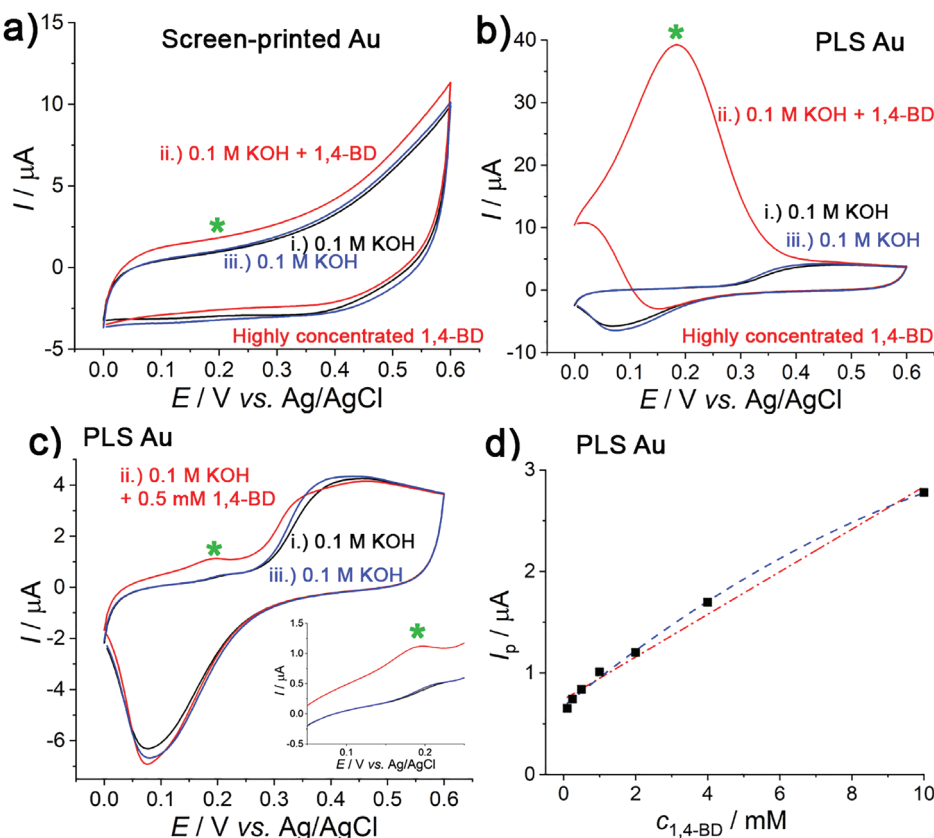| Loading$_{Au}$ [µg cm^{-2}]	t_{Au} [µm][a]	Electrical conductivity [×10^7 S m^{-1}]	% of bulk gold electrical conductivity[b]
472	0.316	0.52	12
944	0.632	0.63	14
1419	0.947	0.72	16

[a] Thickness from SEM measurements of the cross-section of the Au films obtained by blade cutting [b] Electrical conductivity of bulk gold: 4.4×10^7 S m^{-1}.[27]

caused alone by the heat that is generated by the substrate upon irradiation. Gold films were also obtained on a glassy carbon (GC) plate (which is expected to transfer heat much more efficiently than polyimide) and on an ITO-coated glass slide (which hardly absorbs the wavelengths emitted by the used UV lamp) (Section S4, Supporting Information).

The film thickness t scales with the number of printed layers and thus with the amount of gold precursor printed and converted, leading to t_{Au} (µm) $= 6.69 \times 10^4$ µm^3 µg^{-1} $\times$ loading$_{Au}$ (µg µm^{-2}). The density of the Au films was in the range of 13.60 (472 µg$_{Au}$ cm^{-2}) and 15.11 g cm^{-3} (1419 µg$_{Au}$ cm^{-2}), which corresponds to 70% and 78% of bulk gold, respectively (Section S5, Supporting Information). The electrical conductivity ranges from 12% to 16% compared to bulk gold for Au loadings between 472 and 1419 µg$_{Au}$ cm^{-2}, considering the film thicknesses obtained by SEM (**Table 1**, Section S5, Supporting Information). This is well congruent with the electric conductivities of Au films reported in the literature and being obtained with similar concepts. The elec-

trical conductivities of the Au films confirm that once a dense Au coverage is achieved (>340 µg$_{Au}$ cm^{-2}), the electrical conductivity increases only a little with increasing Au loading.

In the following, the electroanalytical performance of an Au film electrode with 634 µm$_{Au}$ cm^{-2} was compared with the performance of a commercial screen-printed Au film electrode. All measurements of these two types of working electrodes were carried out using the same counter electrode (CE) and reference electrode (RE). 1,4-butanediol (1,4-BD), which has been reported to be reasonably well detectable at gold electrodes by electro-oxidation, was herein selected as a test analyte.[28] Apart from its wide use in the chemical industry, 1,4-butanediol has recently found applications for instance in alkaline direct liquid fuel cells.[29] Therefore, there are different areas in which the detection of this analyte by using sensors could be of interest. Among the four stable isomers of butanediol, 1,4-BD is one of the isomers that is relatively difficult to be electrochemically detected, even at gold.[30] This was confirmed by the measurements performed herein with the screen-printed gold electrode. **Figure 7**a shows the CV recorded with a scan rate of 100 mV s^{-1}. The black curve shows the CV of the solution blank (0.1 M KOH), in which capacitive currents due to double-layer charging can be identified. The increase in the current above 0.3 V might be related to the oxidation of Au. The red curve shows the CV of the second measurement with this electrode, which was carried out in 50 mL of 0.1 M KOH to which 0.5 mL of 1,4-butanediol were added. The forward and reverse scans show slightly larger anodic currents all over the potential window, but a clear peak or wave for the electro-oxidation of 1,4-BD cannot be identified. A third measurement was performed, which was a second CV in the blank (0.1 M KOH). The two blanks overlap demonstrating

ADVANCED
SCIENCE NEWS
www.advancedsciencenews.com

ADVANCED
MATERIALS
TECHNOLOGIES
www.advmattechnol.de

Figure 7. The performance of the Au electrodes prepared by PLS in comparison with a standard screen-printed Au electrode in the absence and presence of a test analyte, that is, 1,4-butanediol, in basic aqueous solutions. a,b) CVs in i) 0.1 M KOH (black curves), ii) 0.1 M KOH with a high concentration of 1,4-BD (red), and iii) again in 0.1 M KOH (blue) using a screen-printed Au electrode (a) and an Au electrode obtained by PLS (b). c) Detection of 1,4-BD at low concentrations using the PLS Au electrode: CVs in i) 0.1 M KOH (black), ii) 0.1 M KOH, 0.5 mM 1,4-BD (red), and iii) again in 0.1 M KOH (blue). d) Calibration for the detection of 1,4-BD in 0.1 M KOH using the PLS Au electrode. General notes: Potential scan rate was 100 mV s^{-1}. For all measurements, identical RE and CE were used. The green asterisks show the position of the peak for the electrooxidation of 1,4-BD at the PLS Au electrode.

that the electrode properties were unchanged and that the current increase seen in presence of 1,4-BD was probably related to the electro-oxidation of the analyte. However, the absence of clear peaks demonstrates that this electrode cannot be used for this task. Thereafter, the same series of CV measurements, that is, 0.1 M KOH (1st solution blank), 50 mL 0.1 M KOH + 500 μL 1,4-BD (analyte), and 0.1 M KOH (2nd solution blank), was carried out using the Au film electrode fabricated by PLS (Figure 7b). The CVs in the solution blank show the characteristic shapes in 0.1 M KOH as discussed vide supra, but the measurement in presence of 1,4-BD demonstrates a large anodic peak for the electrooxidation of 1,4-BD. These measurements demonstrate the superior performance of the PLS-fabricated Au electrode compared to a commercial screen-printed Au film electrode. The same observation was made compared with another type of commercial screen-printed Au electrode, in this case, graphite coated with Au NPs (Section S6, Supporting Information).

Thereafter, the PLS Au electrode was used to measure moderate concentrations of 1,4-BD (Figure 7c). The peak currents obtained by measurements in various concentrations of 1,4-BD were extracted without baseline correction in order to create a calibration graph. Linear regression using ISO 8466 resulted in

a calibration line with equation I (μA) = 0.2098 μA mM^{-1} × c (mM) + 0.7384 μA. An r^2 of only 0.9889 was obtained, and consequently, the limit of detection (LOD) was only 1.2 mM. Polynomial fitting was then carried out resulting in equation I (μA) = −0.008 μA mM^{-2} × c^2 (mM^2) + 0.291 μA mM^{-1} × c (mM) + 0.671 μA an r^2 of 0.998. In the investigated concentration interval, no calibration curve could be recorded with the commercial screen-printed Au film electrode demonstrating that Au film electrodes rapidly produced by PLS can outperform certain screen-printed commercial Au electrodes. However, it must be stated that not all commercially available screen-printed electrodes were analyzed in this work.

3. Conclusions

To conclude, inkjet printing and photochemical reduction of an additive-free Au precursor ink for the one-step fabrication of Au films were developed. Inkjet printing was used to create micrometer-thin reaction volumes on a substrate, in which tetrachloroauric(III) acid reduces to pure Au^0, while all other ink components evaporate or degrade leaving no residues on the substrate. By taking advantage of inkjet printing, the loadings of Au

2202039 (10 of 12)

(μg_{Au} cm^{-2}) were highly controllable, either by adjusting the precursor concentration in the ink or, as demonstrated in this work, by the number of droplets deposited per area. The PLS translation rate was optimized so that for each printing pass, the gold precursor conversion into Au^0 was complete.

The performance of the PLS Au electrodes for electroanalytical sensing was evaluated by voltammetric methods in solutions of different pH and the presence of typical electro-active species detectable at gold such as glucose and 1,4-butanediol. The PLS electrodes demonstrated high stability and sensitivity. The sensitivity of PLS Au versus commercial screen-printed Au electrodes was notable and demonstrates not only the competitiveness of PLS for the industrial production of disposable electrochemical sensors but also application advantages. The integration of three electrode sensors for screen printing is a straightforward step and can be fully realized by inkjet printing (Section S7, Supporting Information). The gold sensors could find applications in industrial processes or energy conversion devices in which 1,4-butanediol is used in order to monitor the concentration of 1,4-BD. The combination of an inkjet printer and UV lamp is rather economic compared to other microfabrication techniques used for Au film production. It offers many opportunities for the on-demand production of disposable flexible sensors for research and commercial uses. In fact, inkjet printing constantly develops further approaching more industrial applications, where it can only succeed if it will compete or even overcome certain established state-of-the-art techniques for the fabrication of entire devices or parts thereof. This is in particular valid when a large number of different pattern structures are designed and then printed by depositing scarce and thus expensive materials such as noble metals and noble metal precursors. From the capital cost perspective, inkjet printing can be compared with screen printing (40 000 USD for a research scale platform, noting that the printing process itself does not differ much between laboratory scale and industrial scale inkjet printing and screen printing).[31] The major advantage of inkjet printing is certainly its mask-less and waste-less operation mode, while disadvantages include the stability limits of particulate inks and related printhead lifetimes. Key advantages of the PLS are especially the use of particle-free inks that increase substantially the lifetime of printheads and the use of integrated light sources, operated in-line with printing, rather than using a furnace in a separate process. From the production speed perspective, PLS profits from the use of particle-free inks enabling fast printhead translation times, high jetting frequencies, and the use of parallel nozzles to reduce the printing time, as for the example of the Au patterns presented herein from ≈20 min per pattern to 90 s by changing from 1 nozzle to 16 nozzles.

4. Experimental Section

Materials: Tetrachloroauric(III) acid (HAuCl$_4$ · 3H$_2$O, ≥99.9% trace metals basis), glucose, 1,4-butanediol, isopropanol, 1,2-propanediol, KOH, H$_2$SO$_4$, HClO$_4$, and L-ascorbic acid were obtained from Sigma-Aldrich. A graphene dispersion (graphene ink for inkjet printing with ethyl cellulose in cyclohexanone and terpineol, Sigma-Aldrich), a silver dispersion (30–35 wt% in triethylene glycol monomethyl ether, Sigma Aldrich), and UV curable Bectron IJ 5001 VP (Elantas) were used for inkjet printing of graphene, silver, and a dielectric used as an insulator, respectively. All reagents were used as received. DI water (18.2 MΩ) was produced

by using a Milli-Q water purification system. PI film (150 µm thickness) was obtained from Dr. Dietrich Müller GmbH (Germany). Indium-tin oxide (ITO, In$_2$O$_3$/SnO$_2$)-coated 1 mm thick glass slides (Sigma-Aldrich) and GC Sigradur K plates (HTW) were used as alternative substrates for comparison. Screen-printed Au electrodes (250AT) and screen-printed graphite electrodes modified with Au NPs (110GNP) electrodes were obtained from Metrohm Dropsens.

Print-Light-Synthesis of Gold: The PLS platform was a hybrid system composed of a Fujifilm Dimatix DMP-2831 inkjet printer and an Omnicure S2000 mercury UV lamp (Excelitas). The inkjet printer was operated with printheads in form of cartridges (type DMC-1161, piezoelectric actuation, nominal droplet volume 10 pL, 16 individually addressable nozzles). The printhead holder was customized to enable the mounting of a liquid light guide (output diameter 5 mm) that transferred the light emitted by the UV lamp directly onto the substrate with a spot size of ≈5 mm. The 200 Watt UV lamp yielded outputs of up to 30 W cm^{-2} and was herein used with maximum intensity. The position of the light guide output was close to the nozzles of the cartridges and aligned with the printing direction creating a customized PLS head. The cartridge and the UV light were simultaneously translated during PLS. Therefore, the UV spot passed over the printed area with a minor time shift to irradiate the printed ink quasi-simultaneously. The opening and closing of the shutter of the UV lamp were controlled with the software of the inkjet printer enabling and disabling irradiation on demand.

PLS of Au films were performed by printing a gold precursor ink (tetrachloroauric(III) acid in a mixture of water, isopropanol, and 1,2-propanediol) with varying dpi in various shapes on substrates such as polyimide, glassy carbon, and ITO coated glass slides. The UV lamp was active during each printing pass. The printing speed was adjusted to enable the complete conversion of Au^{III} into Au^0 during each printing pass.

All inkjet printing parameters, such as the waveform for droplet ejection and jetting frequency, were optimized for each ink (Au, graphene, silver, and dielectric). The inks, substrates, and Au films were fabricated and stored under ambient conditions.

Au Characterization: XPS measurements were carried out on an Axis Supra (Kratos Analytical) using the monochromated $K\alpha$ X-ray line of an Aluminum anode. The pass energy was set to 40 eV with a step size of 0.15 eV. The sample was electrically insulated from the stage and charge compensation was used. Data were referenced at 284.8 eV using the aliphatic component of the C1s orbital. XRD measurements were performed with a Bruker D8 Discover Plus equipped with a rotating anode (Cu) and a Dectris Eiger2 500K detector. In order to separate the signal from the different (small) regions on the sample point, collimating optics were used (1 mm pinhole, 1 mm collimator) to select a beam provided by a focusing Göbel mirror. Data were acquired as theta-2theta scans using the 1D mode of the detector. The resistances of the solid Au films were measured either with a collinear four-point-probe measurement system Alessi CPS using osmium probes with a spacing of 1.5875 mm connected to a Keithley 2401 SourceMeter and a collinear four-point probe device with 1 mm separated solid tungsten carbide probes (Jandel Engineering) connected to a Keysight Precision Source/Measure Unit B2902B. Electrochemical measurements were performed using conventional electrochemical workstations, that is, a VersaSTAT 3F (Ametek-Princeton Applied Research), CompactStat (Ivium Technologies), or a CHI900b (CH Instruments). All electrochemical measurements were carried out in a three-electrode configuration using the Au electrodes as WE, a platinum wire as the CE, and miniaturized Ag/AgCl/KCl solution electrodes as RE. For the measurement of the commercial screen-printed electrodes, the contacts of the integrated RE and CE were sealed with scotch tape. Where applied, the normalization of the recorded current was carried out by consideration of the measured geometric surface area of the WE. The thickness of Au films was measured by the inspection of the cross-section of the film using SEM.

Supporting Information

Supporting Information is available from the Wiley Online Library or from the author.

Conflict of Interest

The authors declare no conflict of interest.

Data Availability Statement

The data that support the findings of this study are available from the corresponding author upon reasonable request.

[1] a) Y. Sui, C. A. Zorman, *J. Electrochem. Soc.* **2020**, *167*, 037571; b) B. Hüner, M. Klstl, S. Uysal, İ. N. Uzgören, E. Özdoğan, Y. O. Süzen, N. Demir, M. F. Kaya, *ACS Omega* **2022**, *7*, 40638; c) M. P. Down, E. Martínez-Periñán, C. W. Foster, E. Lorenzo, G. C. Smith, C. E. Banks, *Adv. Energy Mater.* **2019**, *9*, 1803019; d) U. Gulzar, C. Glynn, C. O'Dwyer, *Curr. Opin. Electrochem.* **2020**, *20*, 46.

[2] a) W. Cui, W. Lu, Y. Zhang, G. Lin, T. Wei, L. Jiang, *Colloids Surf., A* **2010**, *358*, 35; b) S. Mekhmouken, N. Battaglini, G. Mattana, A. Maurin, S. Zrig, B. Piro, D. Capitao, V. Noel, *Electrochem. Commun.* **2021**, *123*, 106918; c) M. A. Tabrizi, J. P. Fernández-Blázquez, D. M. Medina, P. Acedo, *Biosens. Bioelectron.* **2022**, *196*, 113729; d) A. Määttänen, P. Ihalainen, P. Pulkkinen, S. Wang, H. Tenhu, J. Peltonen, *ACS Appl. Mater. Interfaces* **2012**, *4*, 955.

[3] a) A. Escudero, L. Gonzalez-Garcia, R. Strahl, D. J. Kang, J. Drzic, T. Kraus, *Inorg. Chem.* **2021**, *60*, 17103; b) D. Wu, B. Yao, S. Wu, H. Hingorani, Q. Cui, M. Hua, I. Frenkel, Y. Du, T. K. Hsiai, X. He, *Adv. Mater.* **2022**, *34*, 2201772.

[4] P. J. Smith, A. Morrin, *J. Mater. Chem.* **2012**, *22*, 10965.

[5] a) V. C. Bassetto, W. O. Silva, C. M. Pereira, H. H. Girault, *J. Solid State Electrochem.* **2020**, *24*, 1781; b) Y. S. Rosen, A. Yakushenko, A. Offenhäusser, S. Magdassi, *ACS Omega* **2017**, *2*, 573.

[6] Y. Zhang, Z. Liang, A. P. Zhang, H. Y. Tam, *Adv. Opt. Mater.* **2021**, *9*, 2001368.

[7] Z. Zhao, J. Bai, Y. Yao, C. Wang, *Mater. Today* **2020**, *37*, 10.

[8] X. Wang, K. Cui, Q. Xuan, C. Zhu, N. Zhao, J. Xu, *ACS Appl. Mater. Interfaces* **2019**, *11*, 21668.

[9] M. Gregorini, R. N. Grass, W. J. Stark, *Ind. Eng. Chem. Res.* **2020**, *59*, 12048.

[10] E. Blasco, J. Müller, P. Müller, V. Trouillet, M. Schön, T. Scherer, C. Barner-Kowollik, M. Wegener, *Adv. Mater.* **2016**, *28*, 3592.

[11] C. Schoner, A. Tuchscherer, T. Blaudeck, S. F. Jahn, R. R. Baumann, H. Lang, *Thin Solid Films* **2013**, *531*, 147.

[12] a) K. Nitta, K. Ishizumi, Y. Shimizu, K. Terashima, T. Ito, *Mater. Chem. Phys.* **2021**, *258*, 123836; b) K. Nitta, Y. Shimizu, K. Terashima, T. Ito, *J. Phys. D: Appl. Phys.* **2021**, *54*, 33LT01.

[13] A. Lesch, *Adv. Mater. Technol.* **2018**, *3*, 1700201.

[14] V. C. Bassetto, M. Mensi, E. Oveisi, H. H. Girault, A. Lesch, *ACS Appl. Energy Mater.* **2019**, *2*, 6322.

[15] W. O. Silva, V. C. Bassetto, D. Baster, M. Mensi, E. Oveisi, H. H. Girault, *ACS Appl. Electron. Mater.* **2020**, *2*, 927.

[16] a) A. Lesch, F. Cortés-Salazar, V. Amstutz, P. Tacchini, H. H. Girault, *Anal. Chem.* **2015**, *87*, 1026; b) Y. He, C. J. Tuck, E. Prina, S. Kilsby, S. D. R. Christie, S. Edmondson, R. J. M. Hague, F. R. A. J. Rose, R. D. Wildman, *J. Biomed. Mater. Res., Part B* **2017**, *105*, 1645.

[17] a) R. García-González, M. T. Fernández-Abedul, A. Pernía, A. Costa-García, *Electrochim. Acta* **2008**, *53*, 3242; b) S. Hassani, M. R. Akmal, A. Salek-Maghsoudi, S. Rahmani, M. R. Ganjali, P. Norouzi, M. Abdollahi, *Biosens. Bioelectron.* **2018**, *120*, 122.

[18] a) E. Gachard, H. Remita, J. Khatouri, B. Keita, L. Nadjo, J. Belloni, *New J. Chem.* **1998**, *22*, 1257; b) V. K. Meader, M. G. John, C. J. Rodrigues, K. M. Tibbetts, *J. Phys. Chem. A* **2017**, *121*, 6742; c) X. Liu, X. Zhang, D. Khakhulin, P. Su, M. Wulff, F. Baudelet, T. C. Weng, Q. Kong, Y. Sun, *J. Phys. Chem. Lett.* **2022**, *13*, 8921.

[19] D. N. Nikogosyan, A. A. Oraevsky, V. I. Rupasov, *Chem. Phys.* **1983**, *77*, 131.

[20] N. Nakashima, K. I. Yamanaka, M. Saeki, H. Ohba, S. Taniguchi, T. Yatsuhashi, *J. Photochem. Photobiol., A* **2016**, *319–320*, 70.

[21] a) L. M. F. Batista, V. K. Meader, K. Romero, K. Kunzler, F. Kabir, A. Bullock, K. M. Tibbetts, *J. Phys. Chem. B* **2019**, *123*, 7204; b) M. Harada, S. Kizaki, *Cryst. Growth Des.* **2016**, *16*, 1200.

[22] B. Derby, *Annu. Rev. Mater. Res.* **2010**, *40*, 395.

[23] a) S. Beyhan, *Int. J. Electrochem. Sci.* **2014**, *9*, 3259; b) S. Beyhan, K. Uosaki, J. M. Feliu, E. Herrero, *J. Electroanal. Chem.* **2013**, *707*, 89; c) D. W. Hwang, S. Lee, M. Seo, T. D. Chung, *Anal. Chim. Acta* **2018**, *1033*, 1.

[24] J. Xu, T. Chen, X. Qiao, Q. Sheng, T. Yue, J. Zheng, *Colloids Surf., A* **2019**, *561*, 25.

[25] M. Pasta, F. L Mantia, Y. Cui, *Electrochim. Acta* **2010**, *55*, 5561.

[26] K. Otto, I. O. Acik, M. Krunks, K. Tõnsuaadu, A. Mere, *J. Therm. Anal. Calorim.* **2014**, *118*, 1065.

[27] D. R. Lide, *CRC Handbook of Chemistry and Physics*, 92nd ed., CRC Press, Boca Raton, FL **2011**.

[28] T. Łuczak, M. Bełtowska-Brzezinska, R. Holze, *J. Appl. Electrochem.* **1993**, *23*, 1039.

[29] K. Waters, D. Nguyen, L. Hernandez, K. Vu, A. Fry-Petit, S. Pecic, J. L. Haan, *J. Power Sources* **2022**, *535*, 231401.

[30] A. Hilmi, E. M. Belgsir, J. M. Le ǵer, C. Lamy, *J. Electroanal. Chem.* **1995**, *380*, 177.

[31] M. Zamani, C. M. Klapperich, A. L. Furst, *Lab Chip* **2023**, *23*, 1410.